

Article

A Single-Stage High-Power-Factor Light-Emitting Diode (LED) Driver with Coupled Inductors for Streetlight Applications

Chun-An Cheng, Chien-Hsuan Chang, Hung-Liang Cheng *, Ching-Hsien Tseng and Tsung-Yuan Chung

Department of Electrical Engineering, I-Shou University, Dashu District, Kaohsiung City 84001, Taiwan; cacheng@isu.edu.tw (C.-A.C.); chchang@isu.edu.tw (C.-H.C.); isu10101001m@cloud.isu.edu.tw (C.-H.T.); isu10001008m@cloud.isu.edu.tw (T.-Y.C.)

* Correspondence: hlcheng@isu.edu.tw; Tel.: +886-7-657-7711 (ext. 6634)

Academic Editors: Shoou-Jinn Chang and Teen-Hang Meen

Received: 31 October 2016; Accepted: 3 February 2017; Published: 10 February 2017

Abstract: This paper presents and implements a single-stage high-power-factor light-emitting diode (LED) driver with coupled inductors, suitable for streetlight applications. The presented LED driver integrates an interleaved buck-boost power factor correction (PFC) converter with coupled inductors and a half-bridge-type series-resonant converter cascaded with a full-bridge rectifier into a single-stage power conversion circuit. Coupled inductors inside the interleaved buck-boost PFC converter sub-circuit are designed to operate in discontinuous conduction mode (DCM) for achieving input-current shaping, and the half-bridge-type series resonant converter cascaded with a full-bridge rectifier is designed for obtaining zero-voltage switching (ZVS) on two power switches to reduce their switching losses. Analysis of operational modes and design equations for the presented LED driver are described and included. In addition, the presented driver features a high power factor, low total harmonic distortion (THD) of input current, and soft switching. Finally, a prototype driver is developed and implemented to supply a 165-W-rated LED streetlight module with utility-line input voltages ranging from 210 to 230 V. Experimental results demonstrate that high power factor (>0.99), low utility-line current THD ($<7\%$), low-output voltage ripples ($<1\%$), low-output current ripples ($<10\%$), and high circuit efficiency ($>90\%$) are obtained in the presented single-stage driver for LED streetlight applications.

Keywords: converter; driver; light-emitting diode (LED); streetlight

1. Introduction

Instead of incandescent bulbs with poor lighting efficiency, light-emitting diode (LED) light sources offer high luminous efficacy, long lamp-life, and are mercury-free alternatives for indoor and outdoor lighting applications [1–3]. Consequently, LEDs has been widely utilized in our daily lives such as streetlights, flashlights, backlight sources, displays, decorative lighting, automotive lighting, and so on [4–16].

Streetlights, which illuminate a road, aim to provide a safe environment during the night-time for motorcycle/bicycle drivers and pedestrians [3,17,18]. Traditional lighting sources for streetlight applications have been high-pressure mercury lamps because of their low-cost. However, high-pressure mercury lamps are not energy efficient. In addition, the discharge tube containing mercury vapors is harmful in terms of polluting our environment when the lamp runs out. Therefore, LEDs have begun to replace the conventional high-pressure mercury streetlight. The conventional two-stage LED driver supplying a rated lamp power of greater than 70 W for streetlight applications, shown

in Figure 1, consists of an input low-pass filter (L_f and C_f) connected with a full-bridge rectifier (D_1, D_2, D_3 and D_4), an interleaved boost power factor correction (PFC) converter (including two capacitors C_{in1} and C_{in2} , two diodes D_{B1} and D_{B2} , two inductors L_1 and L_2 , two power switches S_1 and S_2 , and a DC-linked capacitor C_B), and a half-bridge-type LLC resonant converter (including a Direct-Current (DC)-linked capacitor C_B , two power switches S_3 and S_4 , a resonant capacitor C_r , a resonant inductor L_r , a center-tapped transformer T_1 with two output windings, two output diodes D_5 and D_6 and an output capacitor C_o), along with a LED [19]. Due to two-stage power conversions, the circuit efficiency is limited and more power switches and components are required in the conventional driver.

In response to these challenges, this paper presents and implements a single-stage LED driver with coupled inductors and high power factor for streetlight applications. Descriptions and analysis of operational modes, and design equations of key components in the presented LED driver, and experimental results obtained from a prototype circuit are demonstrated.

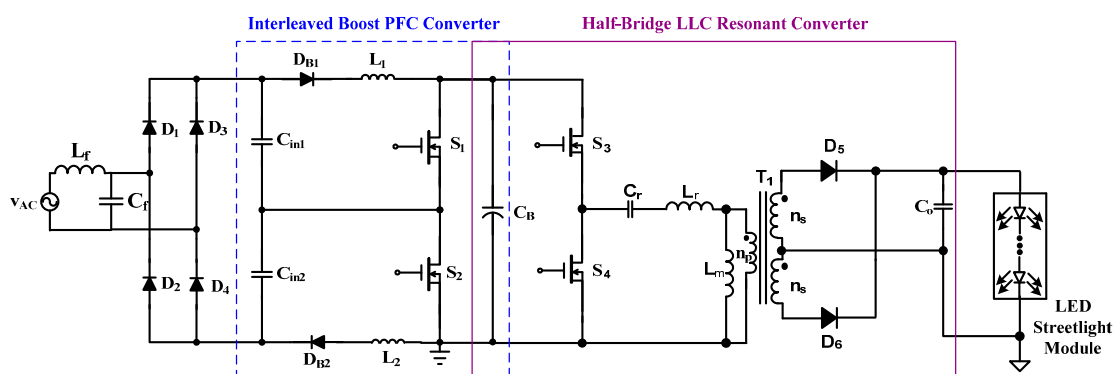


Figure 1. The conventional two-stage light-emitting diode (LED) driver for streetlighting applications, PFC: power factor correction.

2. Descriptions and Operational Modes Analysis of the Presented Single-Stage LED Driver

Figure 2a shows the original two-stage driver circuit suitable for supplying an LED streetlight module, which consists of two buck-boost PFC converters with interleaved operation and a half-bridge-type series resonant converter cascaded with a full-bridge rectifier. The two coupled inductors are employed instead of single-winding inductors in order to accomplish buck-boost conversion. Figure 2b shows the presented LED driver with coupled inductors and interleaved PFC feature by utilizing the synchronous switch technique to simplify power switches and integrate the two-stage configuration into single-stage one. Figure 2b shows the presented LED driver for streetlight applications, which combines an interleaved buck-boost PFC converter with a half-bridge-type series resonant converter cascaded with a full-bridge rectifier into a single-stage power conversion. The interleaved buck-boost PFC converter sub-circuit consists of two capacitors (C_{in1} and C_{in2}), two coupled inductors (L_{B11} and L_{B12} ; L_{B21} and L_{B22}), four diodes (D_{B11} , D_{B12} , D_{B21} , and D_{B22}), two power switches (S_1 and S_2), and a DC bus capacitor (C_{DC}). The half-bridge-type series resonant converter cascaded with a full-bridge rectifier sub-circuit includes a DC bus capacitor (C_{DC}), two switches (S_1 and S_2), a resonant capacitor (C_r), a resonant inductor (L_r), four diodes (D_{o1} , D_{o2} , D_{o3} and D_{o4}), and a capacitor (C_o) along with the LED streetlight module. In addition, coupled inductors (L_{B11} and L_{B12} ; L_{B21} and L_{B22}) are designed to be operated in discontinuous conduction mode (DCM) in order to naturally achieve input-current shaping. In addition, the diodes D_{B12} and D_{B21} are used to block the current going from the utility-line voltage source into the inductors L_{B12} and L_{B21} . Besides, the diodes D_{B11} and D_{B22} are capable of preventing the inductor currents going back to the input capacitors C_{in1} and C_{in2} . Since the input voltage of each buck-boost PFC converter (the voltage on the capacitor C_{in1} or C_{in2}) is half of the utility-line voltage, the peak current of each coupled inductor

and the DC bus voltage will also be half. Because the DC bus voltage is reduced, the presented LED driver is suitable for the applications with high utility-line voltage. Additionally, the input-current harmonics can be reduced by the interleaved operation, so that the size of the input low-pass filter can be miniaturized [20].

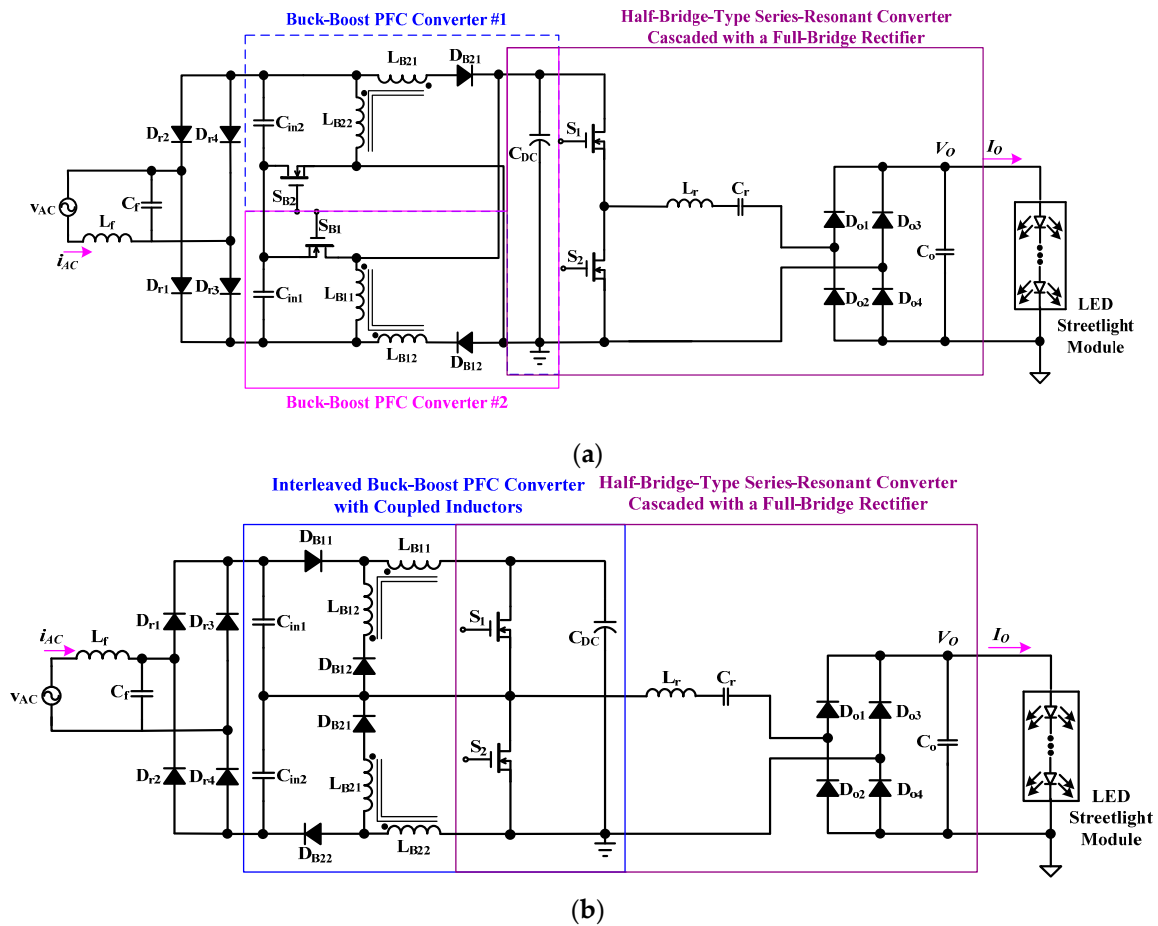


Figure 2. (a) Original two-stage LED driver circuit; (b) the presented single-stage LED driver with coupled inductors and interleaved PFC for streetlight applications.

Figure 3 shows the utilized control circuit diagram of the presented single-stage LED driver for streetlight applications. With using a constant-voltage/constant-current controller (IC1 SEA05) for regulating the LED streetlight module’s output voltage and current, the output LED voltage V_o can be sensed through resistors R_{vs1} , VR_1 and R_{vs2} , and the output LED current can be sensed through resistor R_3 . The sensed output signal from pin 5 of the IC1 feeds into the high-voltage resonant controller (IC3 ST L6599) through a photo-coupler (IC2 PC817). Two gate-driving signals v_{GS1} and v_{GS2} are generated from pin 15 and pin 11, respectively, of the IC3, to carry out regulation of the LED streetlight module’s output voltage and current.

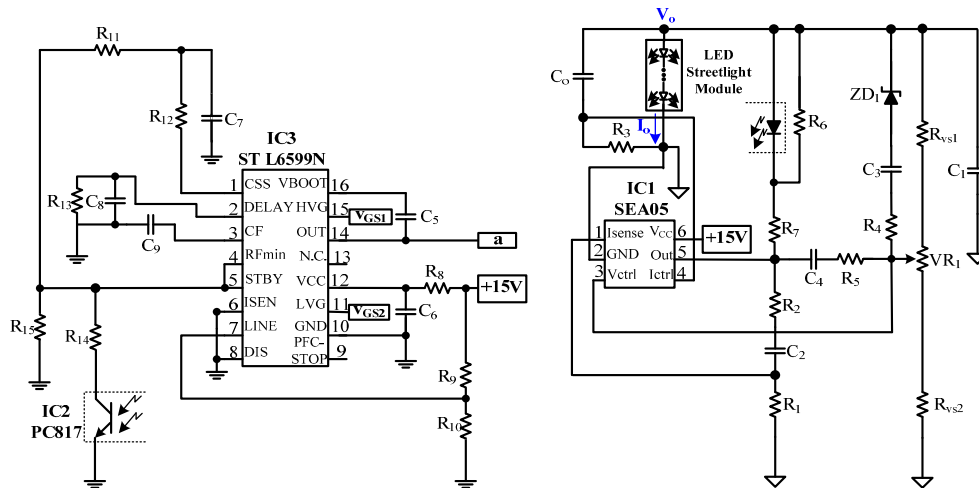


Figure 3. The utilized control circuit of the presented single-stage LED driver for streetlight applications.

Figure 4 presents the simplified circuit of the presented single-stage LED driver for streetlight applications, obtained while analyzing the operational modes. In order to analyze the operations of the presented LED driver, the following assumptions are made.

- (a) Since the switching frequencies of the two switches S_1 and S_2 are much higher than those of the utility-line voltage v_{AC} , the sinusoidal utility-line voltage can be considered as a constant value for each high-frequency switching period.
- (b) V_{REC1} and V_{REC2} , respectively, represent the rectified input voltage sources for the capacitors C_{in1} and C_{in2} .
- (c) Power switches are complementarily operated, and their inherent body diodes and drain-source capacitors (C_{DS1} and C_{DS2}) are considered.
- (d) The conducting voltage drops of diodes D_{B11} , D_{B12} , D_{B21} , D_{B22} , D_{o1} , D_{o2} , D_{o3} and D_{o4} are neglected.
- (e) Coupled inductors (including L_{B11} and L_{B12} ; L_{B21} and L_{B22}) are designed to be operated in DCM for naturally achieving PFC.

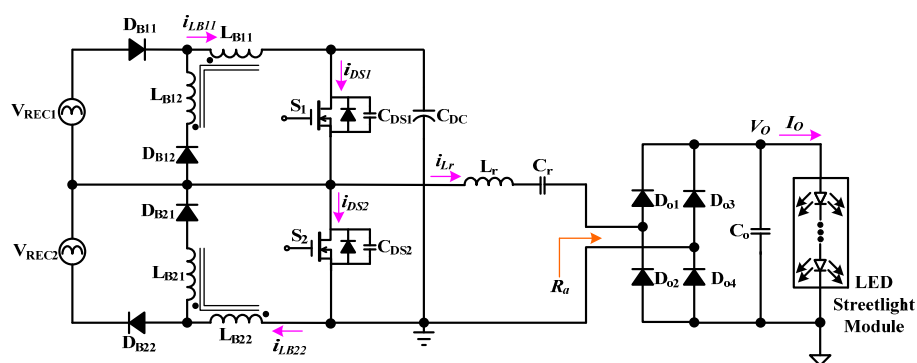


Figure 4. Simplified circuit of the presented single-stage LED driver for streetlight applications.

The operating modes and the key waveform of the presented LED driver for streetlight applications are shown in Figures 5 and 6, respectively, and the analyses of operations are described in detail in the following.

Mode 1 ($t_0 \leq t < t_1$; in Figure 5a): The body diode of switch S_1 is forward-biased at time t_0 , and this mode begins. The resonant capacitor C_r provides energy to the inductor L_r , capacitors C_{DS2} and C_o

and to the LED through diodes D_{o2} and D_{o3} . The diode D_{B21} is forward-biased and coupled inductors L_{B21} and L_{B22} provide energy to capacitor C_{DS2} through diode D_{B21} . At time t_1 , the drain-source voltage v_{DS1} of power switch S_1 is zero and S_1 turns on with zero-voltage switching (ZVS); then this mode ends.

Mode 2 ($t_1 \leq t < t_2$; in Figure 5b): When switch S_1 achieves ZVS turn-on at t_1 , this mode starts. The rectified input voltage source V_{REC1} provides energy to coupled inductor L_{B11} through diode D_{B11} and switch S_1 , and diode D_{B12} is reverse-biased during this mode. The inductor current i_{LB11} linearly increases from zero, and can be expressed as:

$$i_{LB11}(t) = \frac{\left| \sqrt{2}v_{AC-rms} \sin(2\pi f_{AC}t) \right|}{2L_{B11}}(t - t_1), \tag{1}$$

where v_{AC-rms} is the root-mean-square (rms) value of input utility-line voltage, and f_{AC} is the utility-line frequency.

The DC bus capacitor C_{DC} and resonant inductor L_r provide energy to capacitors C_{DS2} , C_r and C_o and to the LED through diodes D_{o1} and D_{o4} . Coupled inductors L_{B21} and L_{B22} continue providing energy to capacitor C_{DS2} through diode D_{B21} . This mode ends when current i_{LB22} decreases to zero at t_2 .

Mode 3 ($t_2 \leq t < t_3$; in Figure 5c): Voltage source V_{REC1} continues providing energy to coupled inductor L_{B11} through diode D_{B11} and switch S_1 . Capacitors C_{DC} and C_{DS2} , along with resonant inductor L_r provide energy to capacitors C_r and C_o and to the LED through diodes D_{o1} and D_{o4} . At t_3 , the coupled-inductor current reaches its peak value, defined as $i_{LB11-pk}(t)$, and is given by:

$$i_{LB11-pk}(t) = \frac{\left| \sqrt{2}v_{AC-rms} \sin(2\pi f_{AC}t) \right|}{2L_{B11}}DT_S, \tag{2}$$

where D and T_S are the duty cycle and period of the power switch, respectively.

This mode ends when diode D_{B12} becomes forward-biased at t_3 .

Mode 4 ($t_3 \leq t < t_4$; in Figure 5d): This mode begins when power switch S_1 turns off at t_3 . The diode D_{B12} is forward-biased and coupled inductors L_{B11} and L_{B12} provide energy to capacitor C_{DS1} . The coupled-inductor current i_{LB11} linearly decreases from its peak level, and can be given by:

$$i_{LB11}(t) = \frac{V_{DC}}{2L_{B11}}(t - t_3), \tag{3}$$

where V_{DC} is the voltage of the DC bus capacitor C_{DC} .

Capacitors C_{DC} and C_{DS2} and resonant inductor L_r continue providing energy to capacitors C_{DS1} , C_r and C_o and to the LED through diodes D_{o1} and D_{o4} . When the drain-source voltage v_{DS2} of S_2 decreases to zero at t_4 , this mode ends.

Mode 5 ($t_4 \leq t < t_5$; in Figure 5e): The body diode of switch S_2 is forward-biased at time t_4 , and this mode begins. The resonant inductor L_r provides energy to capacitors C_{DS2} , C_r and C_o and to the LED through the body diode of power switch S_2 and diodes D_{o1} and D_{o4} . The diode D_{B12} is forward-biased and coupled inductors L_{B11} and L_{B12} provide energy to capacitor C_{DS1} through diode D_{B12} . At time t_5 , the drain-source voltage v_{DS2} of power switch S_2 is zero and S_2 turns on with ZVS; then this mode ends.

Mode 6 ($t_5 \leq t < t_6$; in Figure 5f): When switch S_2 achieves ZVS turn-on at t_5 , this mode starts. The rectified input voltage source V_{REC2} provides energy to coupled inductor L_{B22} through diode D_{B22} and switch S_2 , and diode D_{B21} is reverse-biased during this mode. The DC bus capacitor C_{DC} and resonant capacitor C_r provide energy to inductor L_r , capacitors C_{DS1} and C_o and to the LED through diodes D_{o2} and D_{o3} . Coupled inductors L_{B11} and L_{B12} continue providing energy to capacitor C_{DS1} through diode D_{B12} . This mode ends when current i_{LB11} decreases to zero at t_6 .

Mode 7 ($t_6 \leq t < t_7$; in Figure 5g): Voltage source V_{REC2} continues providing energy to coupled inductor L_{B22} through diode D_{B22} and switch S_2 . The resonant capacitor C_r provides energy to resonant inductor L_r , output capacitor C_o and the LED through diodes D_{o2} and D_{o3} . This mode ends when diode D_{B21} is forward-biased at t_7 .

Mode 8 ($t_7 \leq t < t_8$; in Figure 5h): This mode begins when power switch S_2 turns off at t_7 . The diode D_{B21} is forward-biased and coupled inductors L_{B21} and L_{B22} provide energy to capacitor C_{DS2} . The resonant capacitor C_r continues providing energy to resonant inductor L_r , capacitors C_{DS2} and C_o and to the LED through diodes D_{o2} and D_{o3} . When the drain-source voltage v_{DS1} of S_1 decreases to zero at t_8 , this mode ends. Then Mode 1 begins for the next high-frequency switching period.

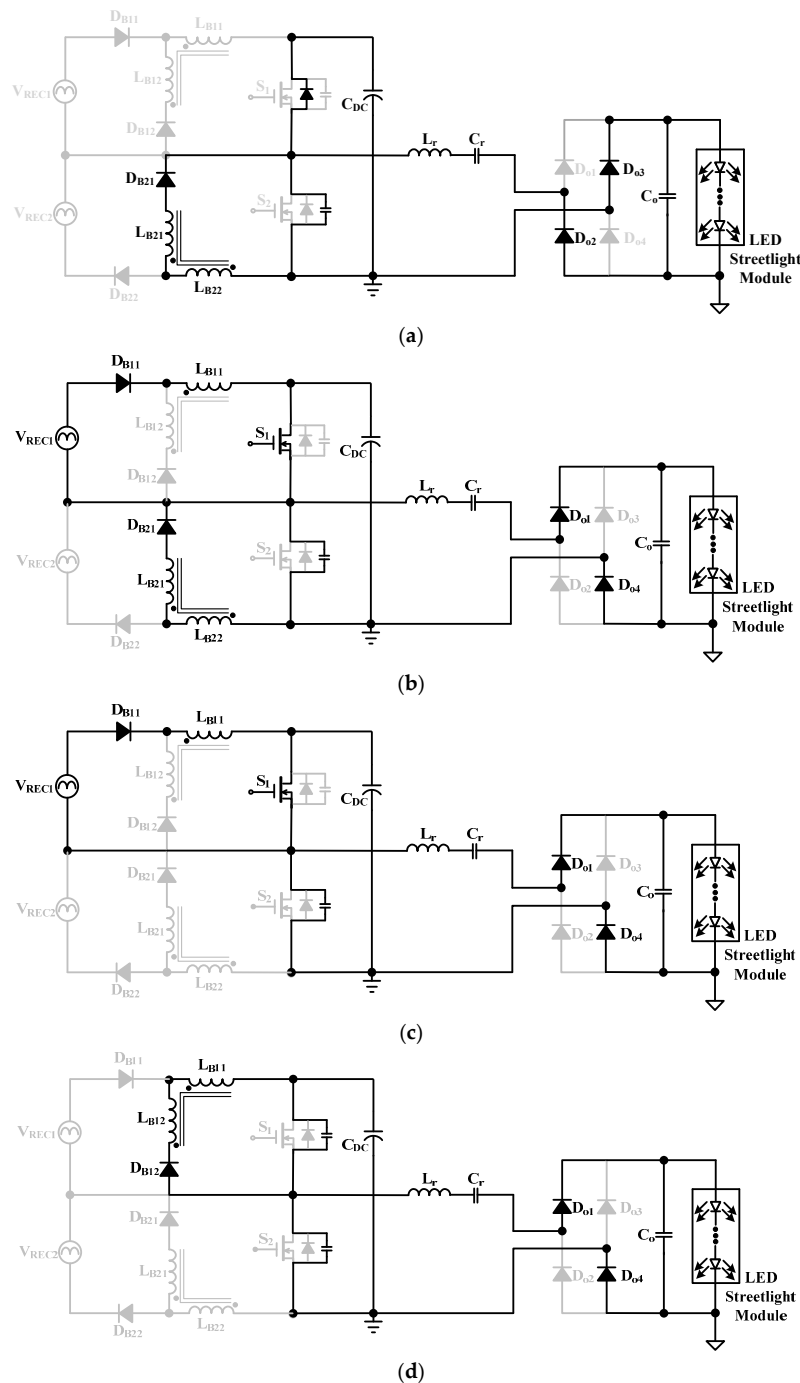


Figure 5. Cont.

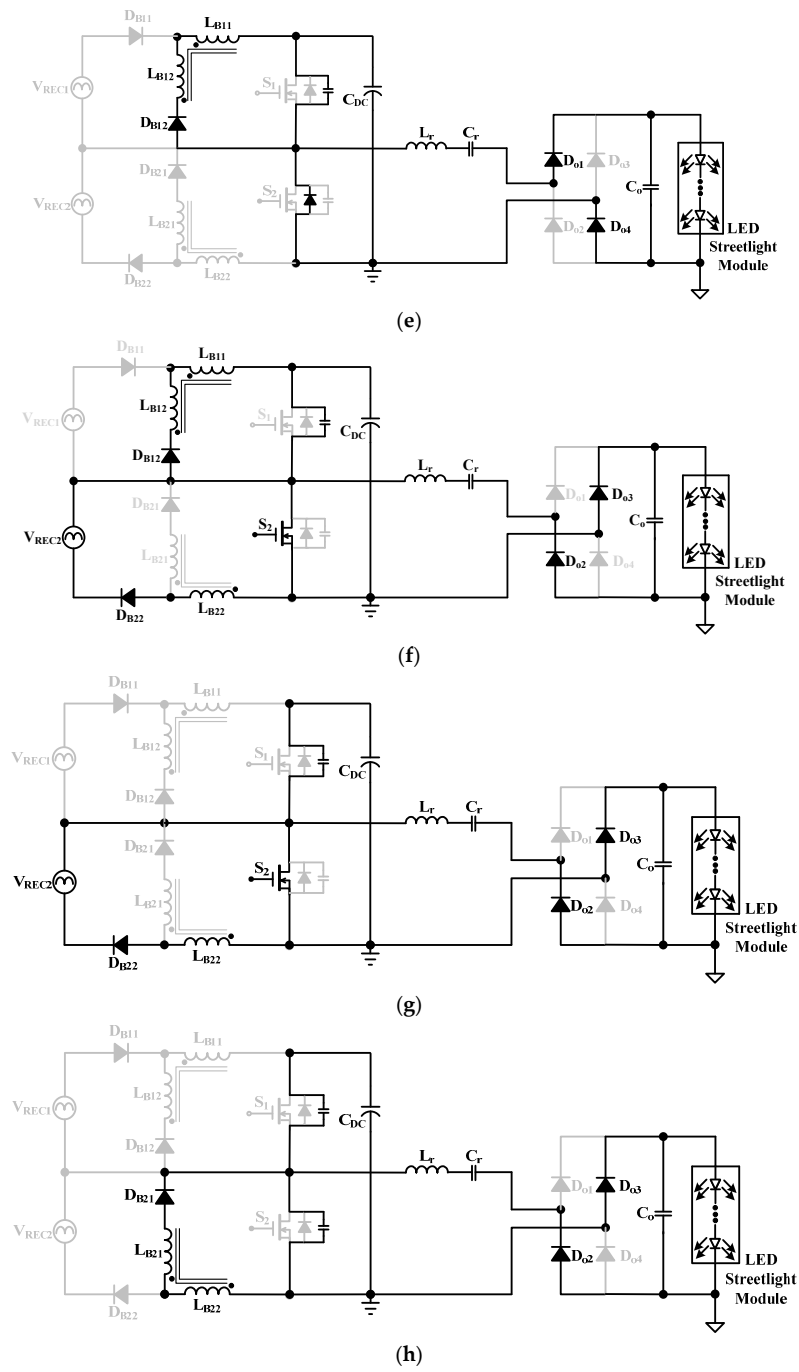


Figure 5. Operation modes of the presented LED driver; (a) Model 1; (b) Model 2; (c) Model 3; (d) Model 4; (e) Model 5; (f) Model 6; (g) Model 7; (h) Model 8.

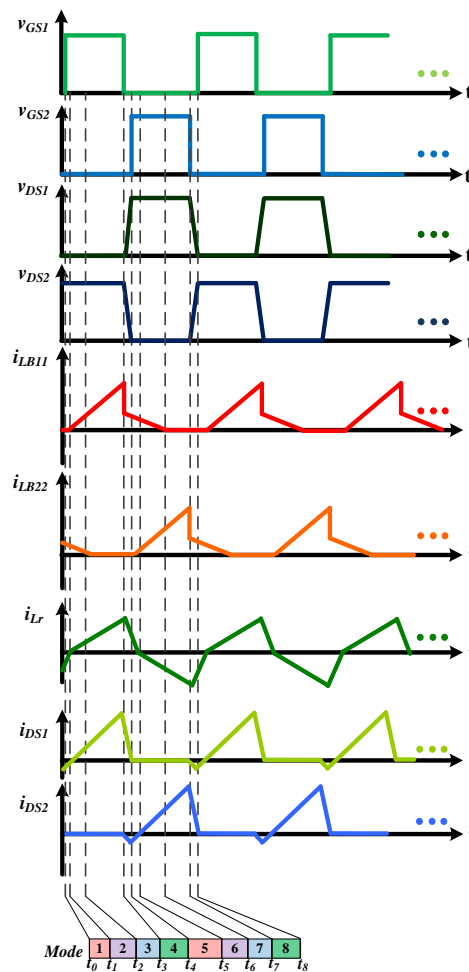


Figure 6. Key waveforms of the presented LED driver for streetlight applications.

3. Design Equations of Key Circuit Components in the Presented LED Driver

3.1. Design of Coupled Inductors L_{B11} , L_{B12} , L_{B21} and L_{B22}

The coupled inductors (L_{B11} and L_{B12} ; L_{B21} and L_{B22}) are designed to be operated in DCM for naturally achieving PFC, and the design equation of them can be expressed as follows [12,20]:

$$L_{B11} = L_{B12} = L_{B21} = L_{B22} = \frac{\eta \cdot v_{ac-pk}^2 \cdot D^2}{4 \cdot f_s \cdot P_o}, \tag{4}$$

where V_{ac-pk} is the peak value of utility-line voltage; η is the estimated efficiency; D is the duty cycle of the power switches; f_s is the switching frequency; and P_o is the output rated power.

In reference to Equation (4) with a η of 0.85, a V_{ac-pk} of $220\sqrt{2}$ V, a D of 0.45, a P_o of 165 W and an f_s of 50 kHz, the coupled inductors L_{B11} , L_{B12} , L_{B21} and L_{B22} are given by:

$$L_{B11} = L_{B12} = L_{B21} = L_{B22} = \frac{0.85 \cdot (220\sqrt{2})^2 \cdot 0.45^2}{4 \cdot 50k \cdot 165} = 505\mu H$$

3.2. Design of Resonant Inductor L_r and Resonant Capacitor C_r

In reference to Figure 2b, the resonant frequency f_r is given by:

$$f_r = \frac{1}{2\pi\sqrt{L_r \cdot C_r}}. \quad (5)$$

The switching frequency f_s is designed to be larger than the resonant frequency f_r so that the resonant tank resembles an inductive network in order to obtain ZVS on for the two power switches [21]. The relationship between the switching frequency f_s and the resonant frequency f_r is selected as:

$$f_s = 4f_r. \quad (6)$$

The quality factor Q_r is defined as:

$$Q_r = \frac{\sqrt{L_r}}{R_a\sqrt{C_r}}, \quad (7)$$

where R_a is the equivalent output resistor referring to the left side of the full-bridge rectifier, and could be expressed by the following equation:

$$R_a = \frac{8V_o}{\pi^2 I_o}. \quad (8)$$

Combining Equation (2) with Equations (3)–(5), the design equations of resonant capacitor C_r and inductor L_r are given by:

$$C_r = \frac{2}{R_a Q_r f_s^2}, \quad (9)$$

and

$$L_r = \frac{4}{\pi^2 f_s^2 C_r}. \quad (10)$$

According to Equation (8), with a V_o of 235 V and an I_o of 700 mA, the equivalent resistor R_a is given by:

$$R_a = \frac{8 \cdot 235}{\pi^2 \cdot 700m} = 272.1\Omega.$$

In reference to Equation (9), with an R_a of 272.1 Ω , the relationship between the resonant capacitor C_r and the switching frequency under different levels of quality factor Q_r is shown in Figure 7. With a Q_r of 0.15 and a switching frequency f_s of 50 kHz, the capacitor C_r is selected to be 1.22 μ F according to Figure 7.

In reference to Equation (10), with a C_r of 1.22 μ F, the resonant inductor L_r is given by:

$$L_r = \frac{4}{\pi^2 \cdot (50k)^2 \cdot 1.22\mu} = 133\mu H.$$

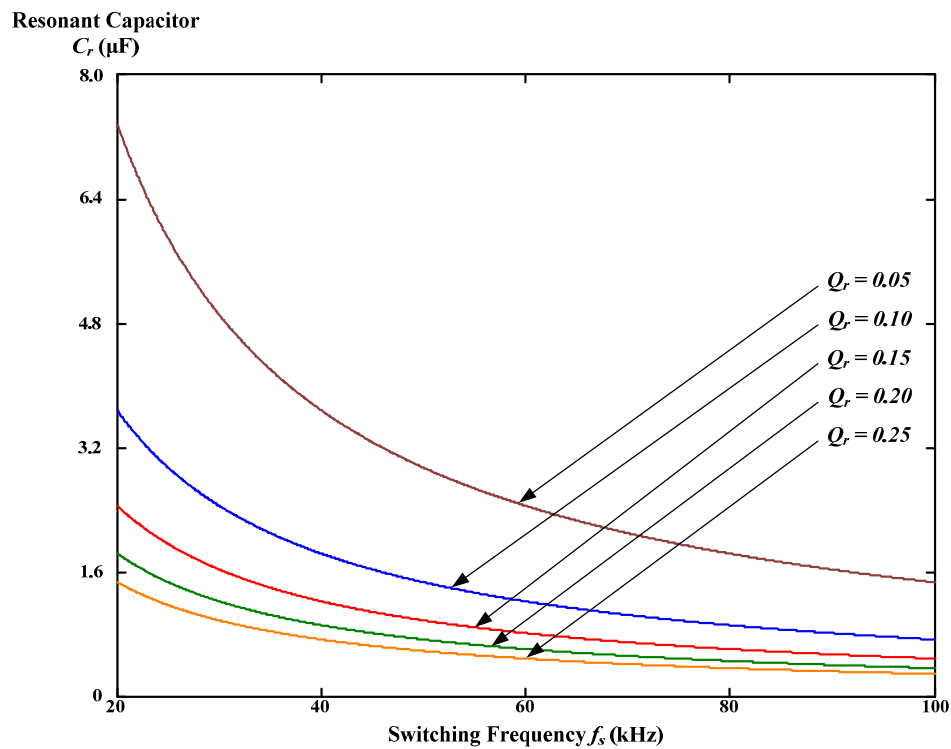


Figure 7. Resonant capacitor C_r versus the switching frequency f_s under different levels of quality factor Q_r .

3.3. Design of Input Low-Pass Filter

The input low-pass filter is composed of an inductor L_f and a capacitor C_f , and the cut-off frequency of the input low-pass filter is given by:

$$f_{cut-off} = \frac{1}{2\pi\sqrt{L_f C_f}} \tag{11}$$

The design consideration of the cut-off frequency in the input low-pass filter is determined to be one-tenth of the switching frequency (which is 5 kHz) in order to filter the high-frequency switching noises. The design equation of the inductor L_f is represented by:

$$L_f = \frac{1}{4\pi^2 f_{cut-off}^2 C_f} \tag{12}$$

On choosing a capacitor C_f of 2 μF (two capacitors of 1 μF in parallel connection), the inductor L_f is given by:

$$L_f = \frac{1}{4\pi^2 f_{cut-off}^2 C_f} = \frac{1}{4\pi^2 (5\text{kHz})^2 2\mu\text{F}} = 2.5\text{mH}$$

4. Experimental Results

A prototype driver has been successfully implemented and tested for powering a 165 W-rated LED streetlight module (LMD003 from AcBel Polytech Inc., New Taipei City, Taiwan) with input utility-line voltages of 220 V \pm 5% (from 210 to 230 V). Tables 1 and 2 show the specifications and key components utilized in the presented single-stage LED driver for streetlight applications, respectively.

Table 1. Specifications of the presented single-stage LED driver.

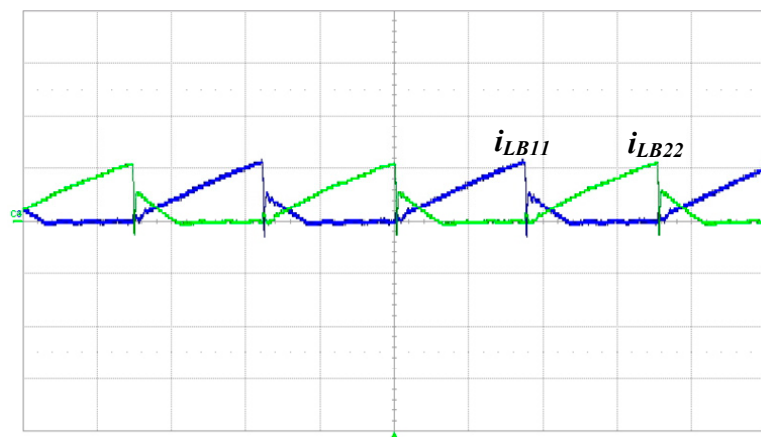
Parameter	Value
Input Utility-Line Voltage v_{AC}	220 V \pm 5% (rms)
Output Rated Power P_O	165 W
Output Rated Voltage V_O	235 V
Output Rated Current I_O	700 mA

Table 2. Key components utilized in the presented LED driver.

Component	Value
Capacitors C_{in1}, C_{in2}	330 nF Component
Inductors $L_{B11}, L_{B12}, L_{B21}, L_{B22}$	505 μ H
Diodes $D_{B11}, D_{B12}, D_{B21}, D_{B22}$	C3D10060
Power Switches S_1, S_2	STP20NM60
DC-Linked Capacitor C_{DC}	100 μ F/450 V
Resonant Inductor L_r	133 μ H
Resonant Capacitor C_r	1.22 μ F
Diodes $D_{o1}, D_{o2}, D_{o3}, D_{o4}$	MUR460
Output Capacitor C_o	220 μ F/400 V
Filter Inductor L_f	2.5 mH
Filter Capacitor C_f	2 μ F

The measured waveforms of coupled inductor currents i_{LB11} and i_{LB22} are shown in Figure 8; both of which have interleaved features and operate in DCM. Figure 9 shows the measured switch voltage v_{DS1} and current i_{DS1} ; Figure 10 presents the measured switch voltage v_{DS2} and current i_{DS2} ; thus, ZVS occurred on both switches for lowering the switching losses.

Figure 11 presents the measured switch voltage v_{DS2} and resonant inductor current i_{Lr} . The current i_{Lr} lags with respect to voltage v_{DS2} so that the series resonant tank resembles an inductive load. Figure 12 depicts the measured output voltage V_O and current I_O ; their average values are approximately 235 V and 0.7 A, respectively. Figure 13 shows measured voltages on the diodes D_{B11} and D_{B22} . The voltage spikes on D_{B11} and D_{B22} are approximately 360 V. In addition, the voltage rating of the diode (C3D10060) is 600 V. Therefore, the utilized diodes are capable of sustaining these voltage spikes. The measured waveforms of input utility-line voltage v_{AC} and current i_{AC} are shown in Figure 14, and the input current is in phase with utility-line voltage, which results in high power factor. In addition, experimental waveforms from Figure 8 to Figure 14 are measured at a utility-line voltage of 220 V.

**Figure 8.** Measured coupled inductor currents i_{LB11} (2 A/div) and i_{LB22} (2 A/div); time scale: 5 μ s/div.

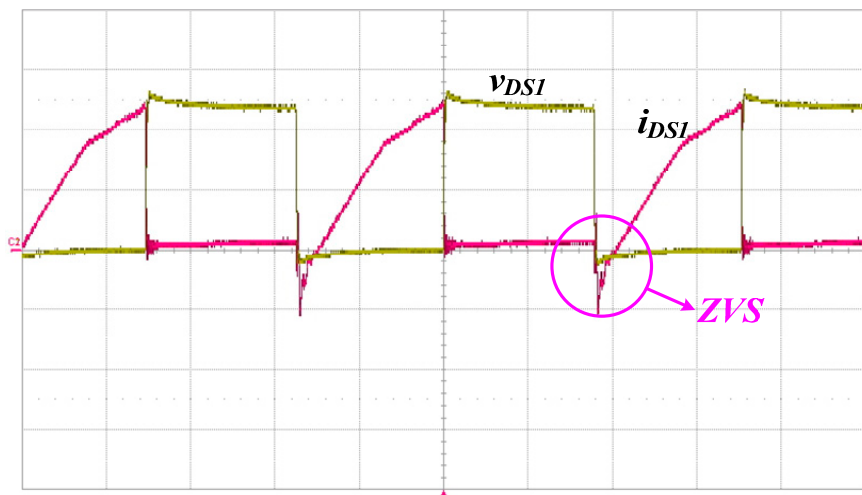


Figure 9. Measured switch voltage v_{DS1} (200 V/div) and current i_{DS1} (2 A/div); time scale: 5 μ s/div.

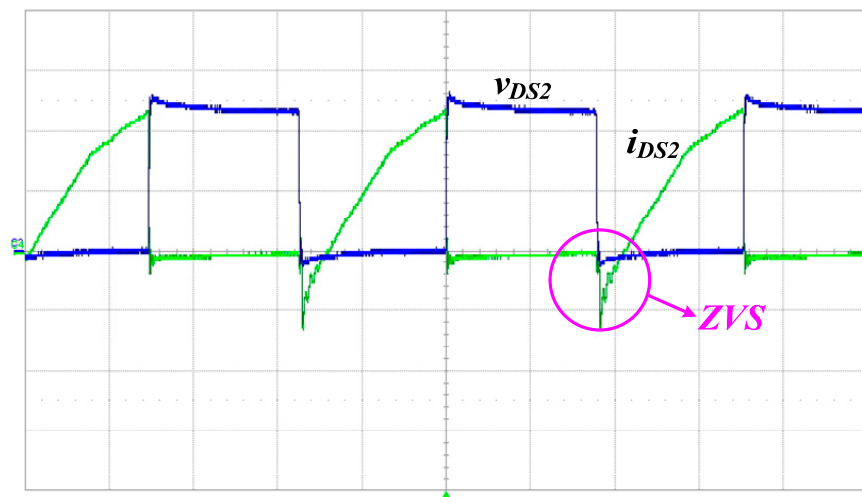


Figure 10. Measured switch voltage v_{DS2} (200 V/div) and current i_{DS2} (2 A/div); time scale: 5 μ s/div.

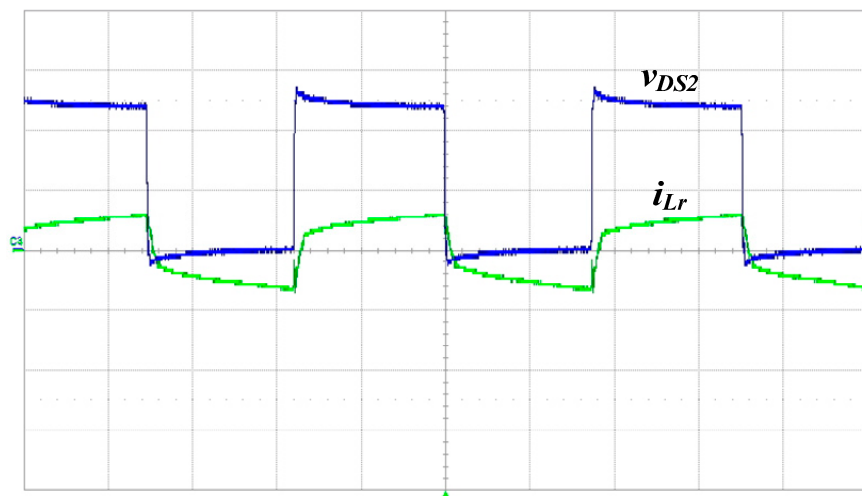


Figure 11. Measured switch voltage v_{DS2} (200 V/div) and resonant inductor current i_{Lr} (2 A/div); time scale: 5 μ s/div.

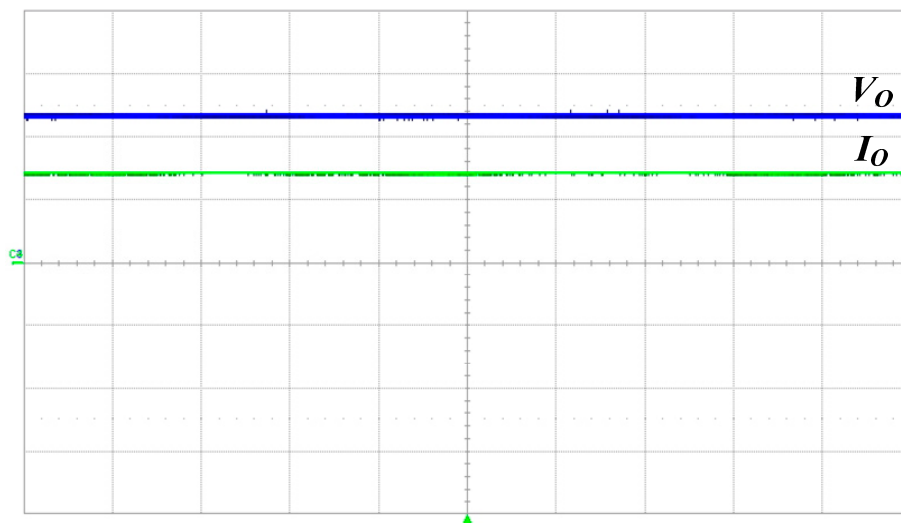


Figure 12. Measured output current I_O (0.5 A/div) and voltage V_O (100 V/div); time scale: 2 ms/div.

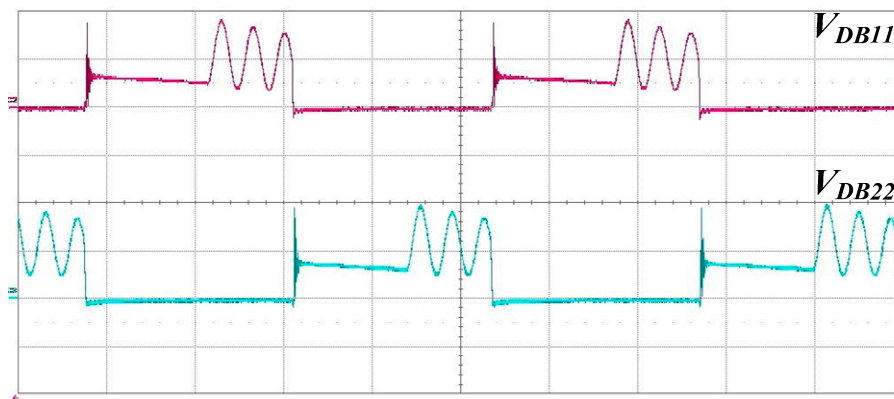


Figure 13. Measured voltages on the diodes D_{B11} and D_{B22} . Voltage scale: 200 V/div; time scale: 5 μ s/div.

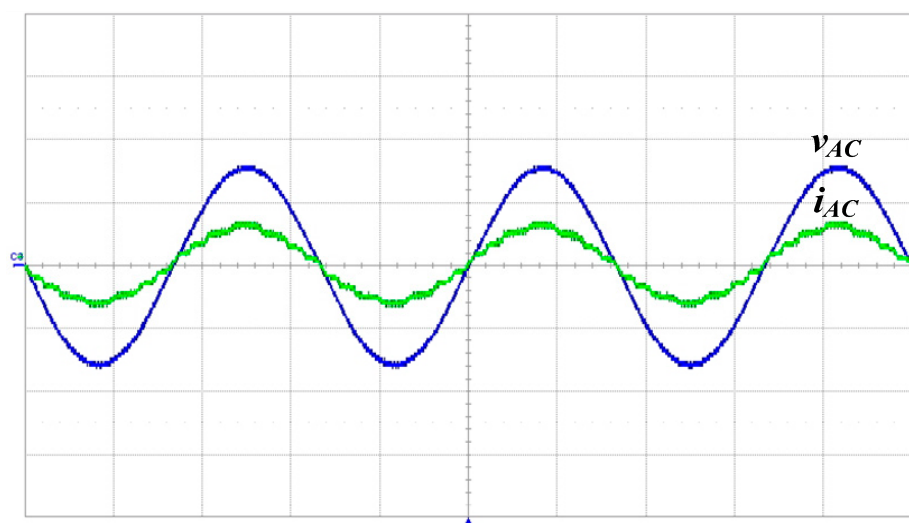


Figure 14. Measured input utility-line voltage v_{AC} (200 V/div) and current i_{AC} (2 A/div); time scale: 5 ms/div.

Figure 15 shows the measured input utility-line current harmonics comparing with the International Electrotechnical Commission (IEC) 61000-3-2 Class C standards at input utility-line voltages ranging from 210 to 230 V, and all current harmonics meet the requirements. Table 3 shows the measured output voltage ripple and current ripple of the presented LED streetlight driver among input voltages ranging from 210 to 230 V; additionally, the output voltage (current) ripple is obtained by the peak-to-peak level divided by the average value of output voltage (current). According to this table, the measured output voltage ripples and current ripples are smaller than 1% and 10%, respectively, during the tested input voltages.

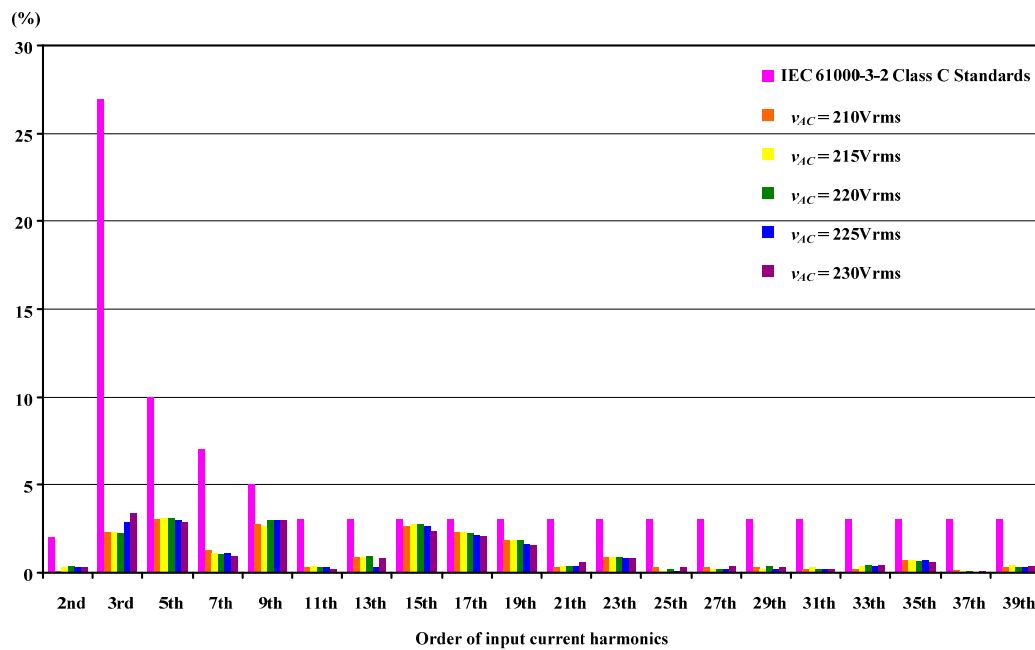


Figure 15. Measured input current harmonics compared with the IEC 61000-3-2 Class C standards.

Table 3. Measured output voltage ripple and current ripple in the presented LED streetlight driver.

Input Voltage (rms)	Voltage Ripple (%)	Current Ripple (%)
210 V	0.75	9.14
215 V	0.75	9.73
220 V	0.79	9.28
225 V	0.75	9
230 V	0.83	8.99

Figure 16 presents the measured power factor and current total-harmonics distortion (THD) of the presented LED driver under utility-line voltages ranging from 210 to 230 V. At a utility-line rms voltage of 220 V, the measured power factor and current THD are 0.992 and 6.55%, respectively. In addition, the measured highest power factor and lowest current THD are 0.993 and 6.5%; these occurred at a utility-line rms voltage of 230 and 210 V, respectively. Figure 17 shows the measured circuit efficiency of the presented LED driver under utility-line voltages ranging from 210 to 230 V; additionally, the measured maximum circuit efficiency is 91.23%, at a utility-line rms voltage of 210 V. In addition, the efficiency which drops with the increase utility-line voltages is related to the voltage gain of the LC series resonant tank. For providing rated output power (voltage/current), the voltage gain of the LC series resonant tank will decrease when the utility-line voltages increase, resulting in an increase in the switching frequency of the power switches. Thus, the switching losses of power switches and conduction losses of power diodes will increase, resulting in lowered circuit efficiency. Figure 18

presents a photograph of supply of the experimental LED streetlight module using the presented driver at a utility-line voltage of 220 V.

Besides, Table 4 shows some measurements of the relationship between output voltage, efficiency and output load current under an input utility-line voltage of 220 V by altering the equivalent load resistor to represent the specific load current. In addition, the measured minimum efficiency is 86.51%, in a minimum load current of 0.3 A. Moreover, Table 5 shows comparisons between the existing single-stage LED driver for streetlight applications in [18] and the proposed one. From Table 5, it can be seen that the proposed LED streetlight driver has better current THD and efficiency than the existing one.

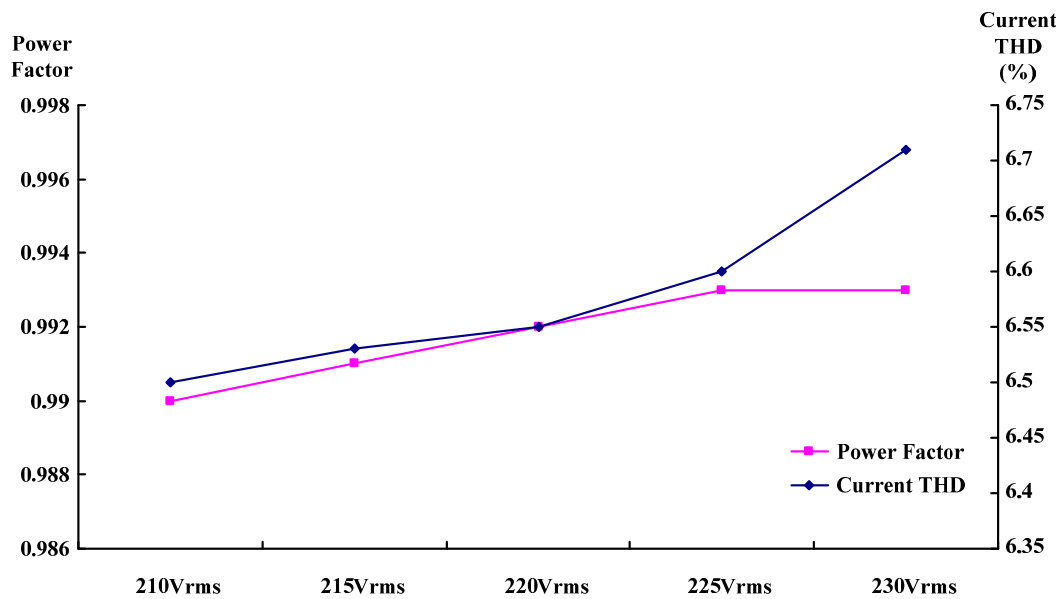


Figure 16. Measured power factor and current total harmonic distortion (THD) under utility-line voltages ranging from 210 to 230 V.

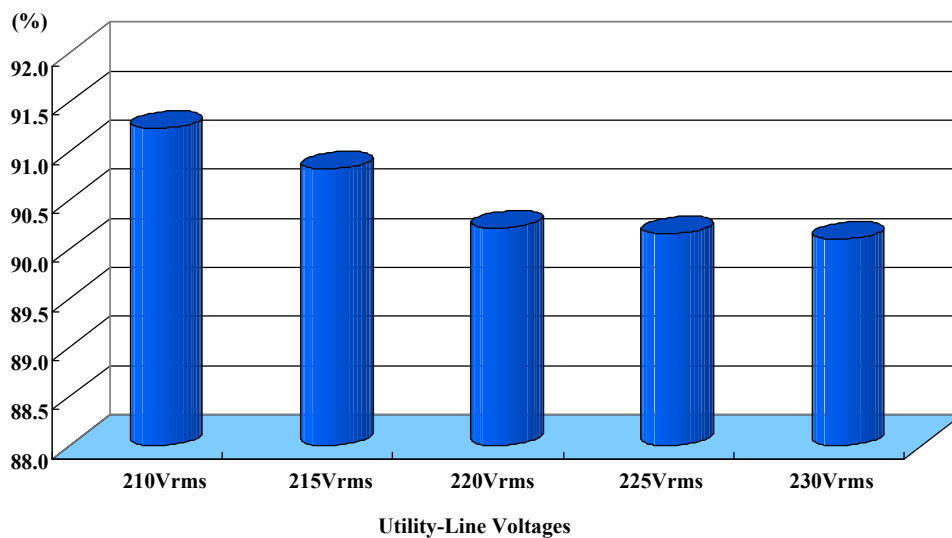


Figure 17. Measured circuit efficiency under utility-line voltages ranging from 210 to 230 V.

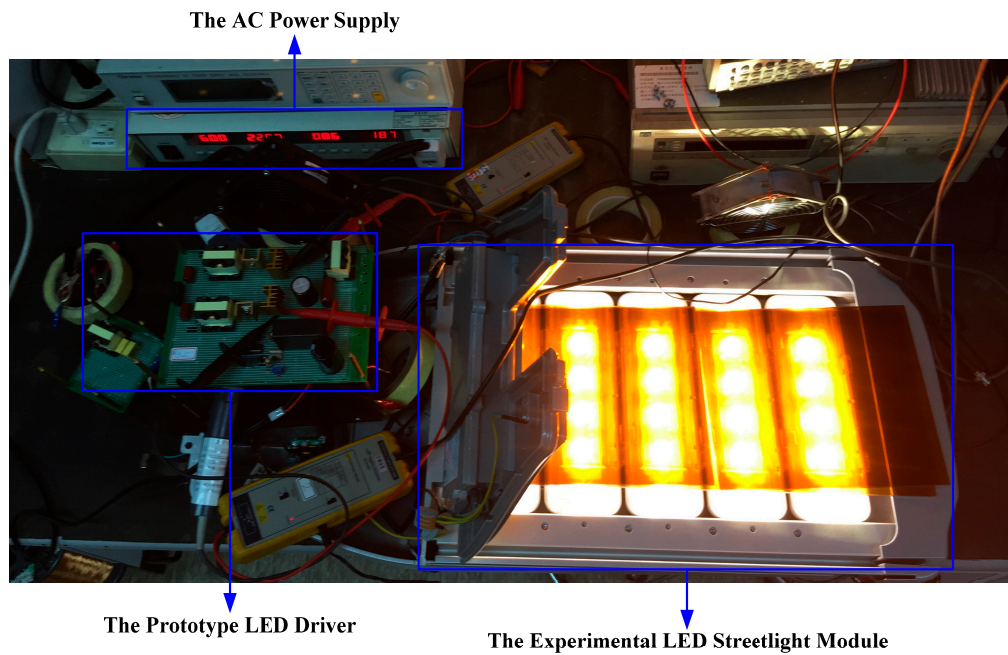


Figure 18. Photograph of supply of the experimental LED streetlight module using the presented driver at a utility-line voltage of 220 V, AC: Alternating-Current.

Table 4. Measured output voltage and efficiency versus output load current under an input utility-line voltage of 220 V.

Output Load Current	0.7 A	0.6 A	0.5 A	0.4 A	0.3 A
Equivalent Load Resistor	336 Ω	392 Ω	470 Ω	588 Ω	783 Ω
Measured Output Voltage	235.31 V	234.91 V	235.31 V	234.86 V	235.34 V
Measured Efficiency	90.22%	89.39%	87.82%	86.59%	86.51%

Table 5. Comparisons between the existing single-stage LED driver for streetlight applications in [18] and the proposed one.

Item	Presented LED Driver in [18]	Proposed LED Driver
Circuit topology	Single-stage (integrating a interleaved boost PFC converter with a half-bridge LLC resonant converter)	Single-stage (integrating a interleaved buck-boost PFC converter with coupled inductors and a half-bridge-type series-resonant converter cascaded with a full-bridge rectifier)
Operating in Utility-Line Voltage Range	90~130 V	210~230 V
Output Rated Power	144 W (36 V/4 A)	165 W (235 V/0.7 A)
Power Switches	2 (S_1, S_2)	2 (S_1, S_2)
Diodes	8 ($D_1 \sim D_6, D_{B1}, D_{B2}$)	12 ($D_{r1} \sim D_{r4}, D_{B11} \sim D_{B22}, D_{o1} \sim D_{o4}$)
Capacitors	6 ($C_f, C_{in1}, C_{in2}, C_B, C_r, C_o$)	6 ($C_f, C_{in1}, C_{in2}, C_{DC}, C_r, C_o$)
Inductors	4 (L_f, L_{B1}, L_{B2}, L_r)	4 (L_f, L_{B11} and L_{B12}, L_{B21} and L_{B22}, L_r)
Transformer	1 (with a magnetic inductor L_m)	0
Measured power factor	0.99 (at 110 V)	0.992 (at 220 V)
Measured current THD	10% (at 110 V)	6.55% (at 220 V)
Measured efficiency	88% (at 110 V)	90.22% (at 220 V)

5. Conclusions

This paper has presented and implemented a single-stage LED driver with a high power factor which is suitable for streetlight applications and integrates an interleaved buck-boost PFC converter with coupled inductors and a half-bridge-type series-resonant converter cascaded with a full-bridge rectifier into a single power conversion stage. A 165-W prototype LED driver has been developed and tested with input utility-line voltages ranging from 210 to 230 V. The experimental results of the presented LED driver display low-output voltage ripple (<1%) and output current ripple (<10%), high power factor (>0.99), low total harmonic distortion of input utility-line current (<7%), zero-voltage switching on power switches, and high circuit efficiency (>90%); thus the functionality of the presented LED streetlight driver is demonstrated.

Acknowledgments: The authors would like to convey their appreciation for grant support from the Ministry of Science and Technology (MOST) of Taiwan under its grant with reference number MOST 104-2221-E-214-012.

Author Contributions: Chun-An Cheng and Chien-Hsuan Chang conceived and designed the circuit; Hung-Liang Cheng performed circuit simulations; Ching-Hsien Tseng and Tsung-Yuan Chung carried out the prototype driver, and measured as well as analyzed experimental results with the guidance from Chun-An Cheng; Hung-Liang Cheng revised the manuscript for submission.

Conflicts of Interest: The authors declare no conflict of interest.

References

1. Schubert, E.F. *Light-Emitting Diodes*; Cambridge University Press: Cambridge, UK, 2006.
2. Energy-Efficient Solutions for Offline LED Lighting and General Illumination. Available online: http://www.mouser.com/pdfDocs/STMicro_OFFLINE-GENERAL_ILLUMINATION_A.pdf (accessed on 5 October 2012).
3. LED Lighting Solutions. Available online: http://www.onsemi.cn/pub_link/Collateral/BRD8034-D.PDF (accessed on 16 March 2013).
4. Liang, T.J.; Tseng, W.J.; Chen, J.F.; Wu, J.P. A novel line frequency multistage conduction LED driver with high power factor. *IEEE Trans. Power Electron.* **2015**, *30*, 5103–5115. [[CrossRef](#)]
5. Chen, Y.S.; Liang, T.J.; Chen, K.H.; Juang, J.N. Study and implementation of high frequency pulse LED driver with self-oscillating circuit. In Proceedings of the 2011 IEEE International Symposium on Circuits and Systems (ISCAS), Rio de Janeiro, Brazil, 15–18 May 2011; pp. 498–501.
6. Moo, C.S.; Chen, Y.J.; Yang, W.C. An efficient driver for dimmable LED lighting. *IEEE Trans. Power Electron.* **2012**, *27*, 4613–4618. [[CrossRef](#)]
7. Cheng, H.L.; Lin, C.W. Design and implementation of a high-power-factor LED driver with zero-voltage switching-on characteristics. *IEEE Trans. Power Electron.* **2014**, *29*, 4949–4958. [[CrossRef](#)]
8. Cheng, H.L.; Chang, Y.N.; Cheng, C.A.; Chang, C.H.; Lin, Y.H. High-power-factor dimmable LED driver with low-frequency pulse-width modulation. *IET Power Electron.* **2016**, *9*, 2139–2146. [[CrossRef](#)]
9. Sauerlander, G.; Hente, D.; Radermacher, H.; Waffenschmidt, E.; Jacobs, J. Driver electronics for LEDs. In Proceedings of the IEEE 41th IAS Annual Meeting, Tampa, FL, USA, 8–12 October 2006; pp. 2621–2626.
10. Hui, S.Y.R.; Qin, Y.X. General photo-electro-thermal theory for light-emitting diodes (LED) systems. *IEEE Trans. Power Electron.* **2009**, *24*, 1967–1976. [[CrossRef](#)]
11. Cheng, H.L.; Lin, C.W.; Chang, Y.N.; Hsieh, Y.C. A high-power-factor LED driver with zero-voltage switching-on characteristics. In Proceedings of the IEEE 10th International Conference on Power Electronics and Drive Systems, Kitakyushu, Japan, 22–25 April 2013; pp. 334–339.
12. Chang, C.H.; Cheng, C.A.; Jinno, M.; Cheng, H.L. An interleaved single-stage LLC resonant converter used for multi-channel LED driving. In Proceedings of the IEEE ECCE-Asia IPEC-Hiroshima, Hiroshima, Japan, 18–21 May 2014; pp. 3333–3340.
13. Sebastian, J.; Lamar, D.G.; Arias, M.; Rodriguez, M.; Hernando, M.M. A very simple control strategy for power factor correctors driving high-brightness LEDs. In Proceedings of the IEEE APEC, Austin, TX, USA, 24–28 February 2008; pp. 537–543.
14. Zhou, K.; Zhang, J.G.; Yuvaraj, S.; Weng, D.F. Quasi-active power factor correction circuit for HB LED driver. *IEEE Trans. Power Electron.* **2008**, *23*, 1410–1415. [[CrossRef](#)]

15. Chang, Y.N.; Kuo, C.M.; Cheng, H.L.; Lee, C.R. Design of dimmable LED lighting driving circuit for battery power source. In Proceedings of the IEEE 10th International Conference on Power Electronics and Drive Systems, Kitakyushu, Japan, 22–25 April 2013; pp. 1168–1172.
16. Cheng, C.A.; Cheng, H.L.; Yang, F.L.; Ku, C.W. Single-stage driver for supplying high-power light-emitting-diodes with universal utility-line input voltages. *IET Power Electron.* **2012**, *5*, 1614–1623. [[CrossRef](#)]
17. Long, X.; Liao, R.; Zhou, J. Development of street lighting system-based novel high-brightness LED modules. *IET Optoelectron.* **2009**, *3*, 40–46. [[CrossRef](#)]
18. Cheng, C.A.; Cheng, H.L.; Chang, C.H.; Yang, F.L.; Chung, T.Y. A single-stage LED driver for street-lighting applications with interleaving PFC feature. In Proceedings of the IEEE International Symposium on Next-Generation Electronics, Kaohsiung, Taiwan, 25–26 February 2013; pp. 150–152.
19. W AC/DC LED Driver. Available online: <http://www.ti.com/lit/ml/slur086/slur086.pdf> (accessed on 15 March 2013).
20. Cheng, C.A.; Chang, C.H.; Cheng, H.L.; Tseng, C.H. A novel single-stage LED driver with coupled inductors and interleaved-PFC. In Proceedings of the IEEE ICPE ECCE-Asia, Seoul, Korea, 1–5 June 2015; pp. 1240–1245.
21. Kazimierczuk, M.K.; Czarkowski, D. *Resonant Power Converters*; John Wiley & Sons, Inc.: Hoboken, NJ, USA, 1995.



© 2017 by the authors; licensee MDPI, Basel, Switzerland. This article is an open access article distributed under the terms and conditions of the Creative Commons Attribution (CC BY) license (<http://creativecommons.org/licenses/by/4.0/>).